

# Impact mechanisms of granular flow against curved barriers

C. E. CHOI\*†, Y. CUI\*, L. H. D. LIU‡, C. W. W. NG\* and S. D. N. LOURENÇO§

Curved seawalls remain one of the most widely adopted coastal-protection measure. A curved face redirects flow momentum and prevents waves from overtopping. Likewise, the use of curvatures for landslide barriers merits investigation given their potential engineering value in reducing the runup height and impact force of geophysical flows. In this study, flume tests were carried out to explore the impact mechanism of dry granular flow against a curved barrier. The impact force, runup height and regime transition path of granular flow for both vertical and curved barriers were compared under different Froude conditions ( $Fr = 4.7$  and  $6.4$ ). The results reveal that in comparison to a vertical barrier, curved barriers reduce the runup height and elongate the duration of impact by up to 17 and 15%, respectively. For curved barriers, the impact force is reduced by up to 25% for coarser granular flows. By contrast, the impact force does not exhibit a significant reduction for finer granular flows. Furthermore, results demonstrate that curved barriers are most suitable for reducing the impact force and suppressing the runup height for more inertial flows, specifically  $Fr > 6.4$  in this study. The phase diagram suggests the curved barrier prompts the transition from airborne jet regime to dead zone regime. The results demonstrate that curved barriers show promising engineering value for mitigating geophysical flows.

**KEYWORDS:** laboratory tests; landslides; model tests; sands; soil/structure interaction

ICE Publishing: all rights reserved

## NOTATION

$C^*$	equivalent drag coefficient
$e$	restitution coefficient
$F$	peak impact force (N)
$Fr$	Froude number
$F_s$	static force after impact (N)
$g$	gravitational acceleration ( $m/s^2$ )
$H_B$	barrier height (m)
$h$	characteristic flow depth (m)
$h_f$	maximum runup height (m)
$K^*$	equivalent earth pressure coefficient
$m$	flow mass (kg)
$P$	peak impact pressure of flow (Pa)
$t$	duration of impact process (s)
$v$	average flow velocity (m/s)
$\alpha$	dynamic load coefficient
$\delta$	characteristic particle diameter (m)
$\theta$	channel inclination ( $^\circ$ )
$\rho$	bulk density ( $kg/m^3$ )
$\rho_f$	bulk density of debris flow in contact with barrier ( $kg/m^3$ )
$\rho_i$	bulk density of upstream flow ( $kg/m^3$ )
$\phi$	interface friction angle ( $^\circ$ )

## INTRODUCTION

Curved seawalls suppress the runup height by redirecting flow momentum back towards the sea (Kamikubo *et al.*,

2003; Anand & Sundar, 2016). Similarly, barriers with curved geometries have been proposed by Kwan (2012) to suppress the runup of geophysical flows (Fig. 1). However, the recommended geometry is empirical and its performance has remained unclear. Despite similarities in curved barriers for coastal protection and mitigating geophysical flows, guidelines (de Rouck *et al.*, 2004, EurOtop, 2016) cannot be assumed to be mutually applicable. This is because wave loading is continuous and dynamics are influenced by viscous forces (Ng *et al.*, 2016). By contrast, geophysical flows, comprise a granular assembly (Forterre & Pouliquen, 2011) whereby grain stresses control flow dynamics (Iverson & Vallance, 2001; Iverson & George, 2014; Iverson, 2015). Furthermore, granular deposits accumulate at the base of the barrier, called a dead zone (Gray *et al.*, 2003). This dead zone contributes static loading to the barrier and redirects the momentum of subsequent flow vertically along the barrier. The formation of dead zone complicates the interaction between geophysical flows and a structure (Faug *et al.*, 2002; Ng *et al.*, 2017a).

Aside from installing curvatures at the barrier crest, Song *et al.* (2017), Koo *et al.* (2017), reported that changes in geometry at the base of the barrier can likewise alter impact flow kinematics and dynamics. More specifically, the formation of a ramp-like dead zone comprising granular deposits at the base of the barrier is very effective at redirecting flow momentum vertically along the barrier rather than into the barrier. Ng *et al.* (2017c) reported that dead zones reduce impact loading by 30% at the upper parts of a barrier. Given the added-benefits, there is certainly potential in enhancing the design of barriers against geophysical flows by altering barrier geometry.

The impact load of geophysical flows against barriers is estimated using a momentum-based approach (Mizuyama, 1979; Hungr *et al.*, 1984; VanDine, 1996)

$$P = \alpha \cdot \rho v^2 \quad (1)$$

Manuscript received 28 June 2017; first decision 19 November 2017; accepted 20 November 2017.

Published online at [www.geotechniqueletters.com](http://www.geotechniqueletters.com) on 22 December 2017.

\*Department of Civil Engineering, the Hong Kong University of Science and Technology, Hong Kong, China.

†The HKUST Jockey Club Institute for Advanced Study, Hong Kong, China.

‡Department of Civil Engineering, the Hong Kong University of Science and Technology, Hong Kong, China (Orcid:0000-0002-5772-0653).

§Department of Civil Engineering, the University of Hong Kong, Pokfulam Road, Hong Kong, China.

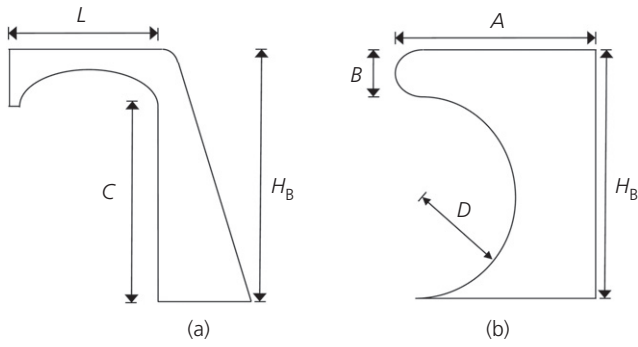


**Fig. 1.** (a) Debris-flow deflector (Kwan, 2012) and (b) curved sea wall design recommendations (Thorn & Roberts, 1981)

where  $P$  is the impact pressure,  $v$  the average flow velocity,  $\rho$  the bulk density of flow,  $\alpha$  is a dynamic coefficient accounting flow composition and barrier type. The dynamic load coefficient  $\alpha$  can range from 1.0 to 2.5 in literature (Mizuyama, 1979; Hungr *et al.*, 1984; Kwan, 2012) and can be characterised as function of the Froude ( $Fr$ ) conditions. More specifically,  $\alpha = 5.3Fr^{-1.5}$  (Hübl *et al.*, 2009; Cui *et al.*, 2015). Faug (2015a, 2015b) proposed a scaling argument to demarcate the value of  $\alpha$  over a broad  $Fr$ . The analytical expression is given as

$$\alpha = C^* + \frac{K^*}{Fr^2} \quad (2)$$

$$C^* = 2\beta \left( 1 - \frac{[1 - (1 - e/\pi/2)(\theta - \phi)] \cos \theta}{\cos \phi} \right) \quad (3)$$

$$K^* = k + \frac{H}{h} \left( 2 + \frac{H}{h} \right) (1 + \tan \theta \tan \phi) \quad (4)$$

where  $C^*$  is the equivalent drag coefficient and  $K^*$  the equivalent earth pressure coefficient. The value of  $C^*$  and  $K^*$  can be determined through the inclination angle  $\theta$ , friction angle  $\phi$ , restitution coefficient  $e$ , velocity gradient  $\beta$  and classical earth pressure coefficient  $k$  (Faug *et al.*, 2012).

Aside from impact, potential runup of geophysical flows against vertical barriers needs to be considered to ensure over spilling does not occur (Choi *et al.*, 2015). Two commonly adopted approaches for predicting runup on vertical barriers are proposed by Kwan (2012) and Jóhannesson *et al.* (2009). The former approach is an energy-based approach, which is a conversion of inflow kinetic energy into potential energy under the assumption that no energy is dissipated

$$\frac{h_f}{h} = 1 + \frac{v^2}{2gh} \quad (5)$$

where  $h_f$  is the runup height,  $h$  the flow depth and  $g$  is the gravitational acceleration. Jóhannesson *et al.* (2009) and Albaba *et al.* (2017) proposed an approach based on the formation of a hydraulic jump that propagates backward. The conservation of mass and momentum is considered across the section of the jump discontinuity

$$\left( \frac{h_f}{h_i} \right)^3 + A \left( \frac{h_f}{h_i} \right)^2 - B \left( \frac{h_f}{h_i} \right) + C = 0 \quad (6)$$

where  $\rho_f$  and  $\rho_i$  are the flow densities in contact with the barrier and just upstream of the barrier, respectively,  $A = (1/\lambda_\phi)$ ,  $B = -(1 + 2Fr^2)/\lambda_\phi$ ,  $C = (1/\lambda_\phi^2)$  and  $\lambda_\phi$  is defined as the density ratio of granular flow before impact and after

impact (Albaba *et al.*, 2017). The performance of these approaches when examining barriers with varying geometries warrants further investigation.

For describing the granular patterns formed when granular flow impacts a vertical barrier down an incline, a phase diagram was proposed by Faug (2015b). The phase diagram identifies four granular patterns using Froude number ( $Fr$ ) and the ratio of barrier height and flow depth ( $H_B/h$ ). These patterns include: (i) granular airborne jet regime at high  $Fr$  and low  $H/h$ . During this regime, the incoming flow is able to easily overflow the wall and form a long overflow trajectory. (ii) Granular dead zone regimes happen at intermediate values of  $Fr$  and low  $H/h$ . In this regime, a quasi-static stagnant zone coexists overflow. (iii) Granular jumps regimes occur at high  $Fr$  and high  $H/h$ . In this regime, the incoming flow has high kinetic energy, but the potential energy associated with the barrier height is also high. Therefore, a granular bore forms and is able to propagate upstream and interact with the incoming flow. (iv) At certain conditions, a stationary granular jump can be formed where part of the incoming flow overtops the wall, forming a jet of very low energy. However, the effect of a curved barrier on the transition of the granular regime during the flow-barrier interaction remains unfathomed. To advance the understanding of geometry effects on flow-barrier interaction, the regime transition of granular flow-varying barrier geometries merits further investigation.

In this study, a series of flume experiments were conducted to investigate impact mechanisms of granular flow against curved barrier. The impact force and runup height of granular flows against vertical and curved barrier under different  $Fr$  were investigated. The transition of granular patterns to different barrier geometries was compared.

## FLUME MODELLING

A 5 m long rectangular flume model (Fig. 2) was used in this study (Choi *et al.*, 2016). The channel has a width and a depth of 0.2 and 0.6 m, respectively. The channel is inclinable from 0 to 40°. The storage container has a maximum storage capacity of 50 kg. A steel plate with a height, width and thickness of 100, 200 and 10 mm, respectively, was installed orthogonally to the channel at the distance of 1200 mm from the gate. The vertical and curved barriers were mounted on the plate for impact tests (Fig. 3).

## Scaling

Granular flows are characterised using the ratio between the characteristic particle diameter and the flow depth,  $\delta/h$ , which ranges from 0.02 to 0.11 in this study. This parameter principally governs the grain stresses of granular flow, whether the flow behaves in a contact-dominated or shear-dominated manner (Ng *et al.*, 2017b). Furthermore, the dynamics of the flow are characterised using the Froude number ( $Fr$ ), governing open-channel flow and the interaction with structures (Hübl *et al.*, 2009; Zhou & Ng, 2010; Armanini *et al.*, 2011; Choi *et al.*, 2015; Cui *et al.*, 2015; Faug, 2015a). The  $Fr$  is the ratio of inertial forces to the gravitational forces

$$Fr = \frac{v}{\sqrt{gh \cos \theta}} \quad (7)$$

where  $\theta$  is the channel inclination. Natural geophysical flows can be characterised using  $Fr$  from 0.5 to 7.6 (Hübl *et al.*, 2009; Cui *et al.*, 2015). By varying the channel inclination from 20° to 40°,  $Fr$  from 4.7 to 6.4 is achieved.

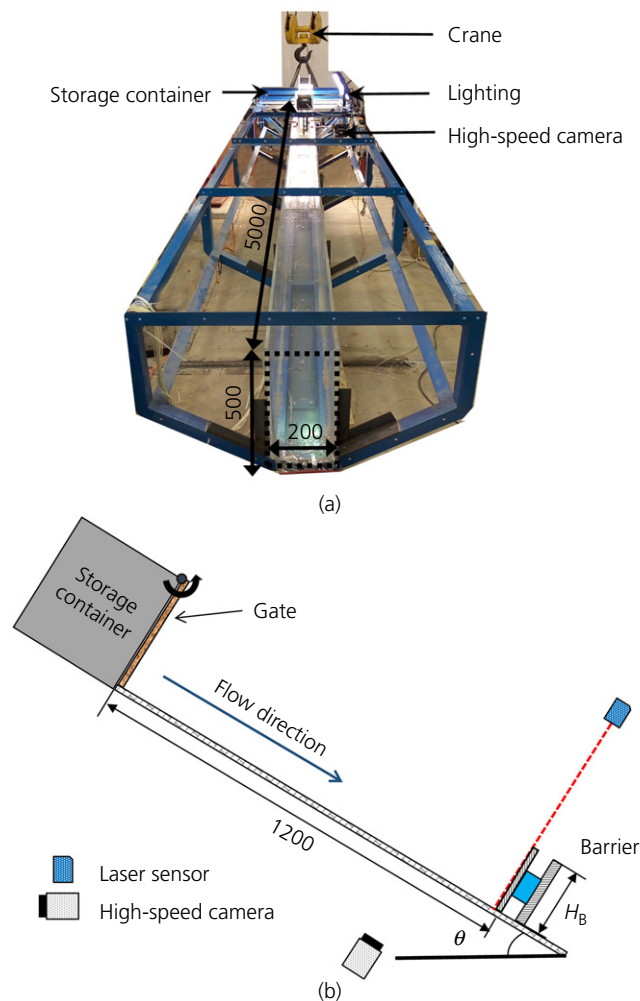


**Fig. 2.** Flume model and instrumentation set-up: (a) front view; (b) schematic side view (all dimensions in millimetres)

### Instrumentation

Figure 2(b) shows a schematic side view of the instrumentation set-up. Two high-speed cameras (model: Mikrotron MotionBLITZ EoSens mini2) were used to capture the impact kinematics. The high-speed cameras captured images at a sampling rate of 640 frames/s at a resolution of  $1400 \times 1600$  pixels. The high-speed camera settings enable the interpretation of velocity fields using particle image velocimetry (PIV) (White *et al.*, 2003). Each image recorded was compartmentalised into a grid of test patches. The displacement vector of each patch between images was traced by locating the peak of an autocorrelation function.

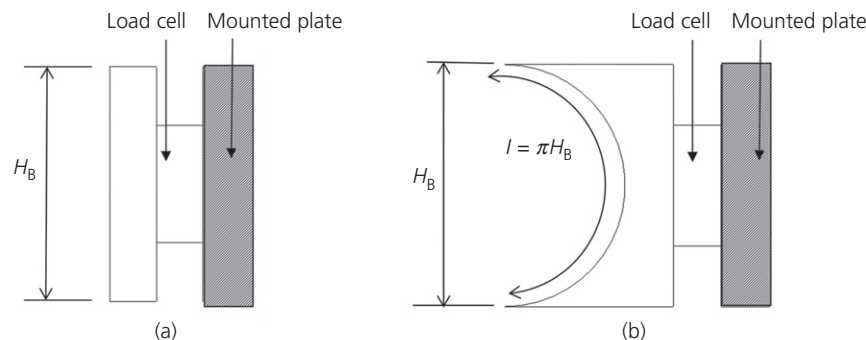


**Fig. 3.** Schematic side view: (a) vertical barrier; (b) curved barrier

The accuracy of this technique is reported as  $\pm 0.057$  m/s (Choi *et al.*, 2016). A laser sensor (model: Wenglor YT44MGV) was installed on the top of the flume to measure changes in flow depth just upstream from the barrier. The set-up to measure impact force is showed in Fig. 3. The impact force is measured using a load cell (model: Kyowa LUX-B-200ID) at a sampling rate of 2 kHz. It is fastened to the rigid plate mounted on the flume. The load cell is connected to a data logger (cDAQ Controller, 1.91 GHz Quad-Core Atom) for data acquisition. The physical properties of barriers are summarised in Table 1.

### Test programme

Two types of barriers were investigated, specifically vertical and curved barriers. Leighton Buzzard Fraction C sand with characteristic diameters of 0.6 mm and glass spheres with characteristic diameters of 3.0 mm were adopted for this study. As aforementioned,  $Fr$  of the flow before impacting the barrier was varied by adjusting the channel inclination as 20, 30 and 40°. To characterise  $Fr$ , free flow tests without a barrier in the channel were performed for each combination of particle size and channel inclination (Fig. 4). In these free flow tests, the velocity and flow depth were measured to characterise  $Fr$  at the position along the flume where the barrier would be installed. After the  $Fr$  conditions were characterised for a particular channel inclination and particle diameter, impact tests were conducted with vertical and curved barriers. To ascertain the repeatability of each impact test, the characteristics of the flow front before impact (Fig. 5) were examined. The difference of velocity between each test is within 0.543%. The difference of flow depth is within 7.8%. The material parameters for the granular material are summarised in Table 2 and the test programme is summarised in Table 3.

## INTERPRETATION OF RESULTS

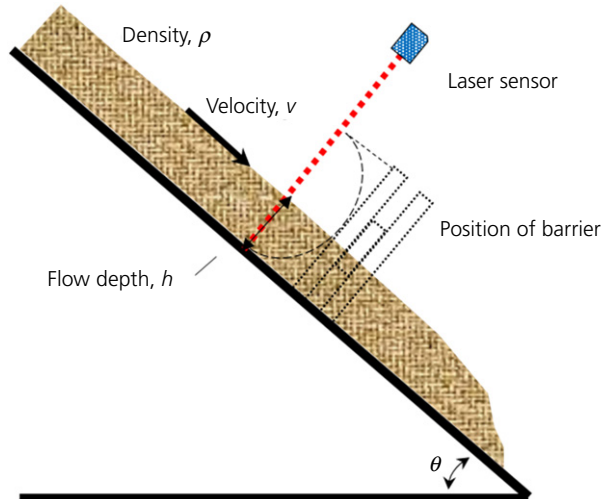
### Impact kinematics

Figures 6 and 7 show the impact kinematics of coarser granular flow against vertical (test V-G3-I40) and curved barriers (test C-G3-I40) at an inclination of 40°, respectively. Captured kinematics are shown on the left and the corresponding PIV analyses (White *et al.*, 2003) is shown on the right. The flow direction is towards the right and the maximum deduced velocities are also shown for each snapshot.

The granular flow comprising coarser grains (test V-G3-I40) forms a thin wedge-like front and impacts the vertical barrier at  $t = 10.0$  s with a velocity of 2.03 m/s (Fig. 6(a)). Runup is observed along the barrier surface (Fig. 6(b)) and the flow velocity decreases by 5% after initial impact. The subsequent flow material impacts and piles up

**Table 1.** Physical properties of barrier

Barrier type	Vertical barrier	Curved barrier
Curvature: rad	0	$\pi$
Mass: kg	0.54	0.62
Young's modulus: GPa	69	69
Bulk density: kg/m <sup>3</sup>	2700	2700

**Fig. 4.** Schematic side view of control test to obtain Froude condition

on top of the existing deposits, forming a dead zone at the base of the barrier. The dead zone enlarges as layers of granular flow accumulate. The ramp-like dead zone eventually transfers momentum of subsequent flow vertically along the barrier rather than into the barrier. The maximum runup height is reached at  $t = 10.4$  s (Fig. 6(c)). At  $t = 11.0$  s, the retention capacity of the barrier is reached and flow cascades over the barrier (Fig. 6(d)). The velocity of the granular flow is further reduced by 29% compared with initial conditions.

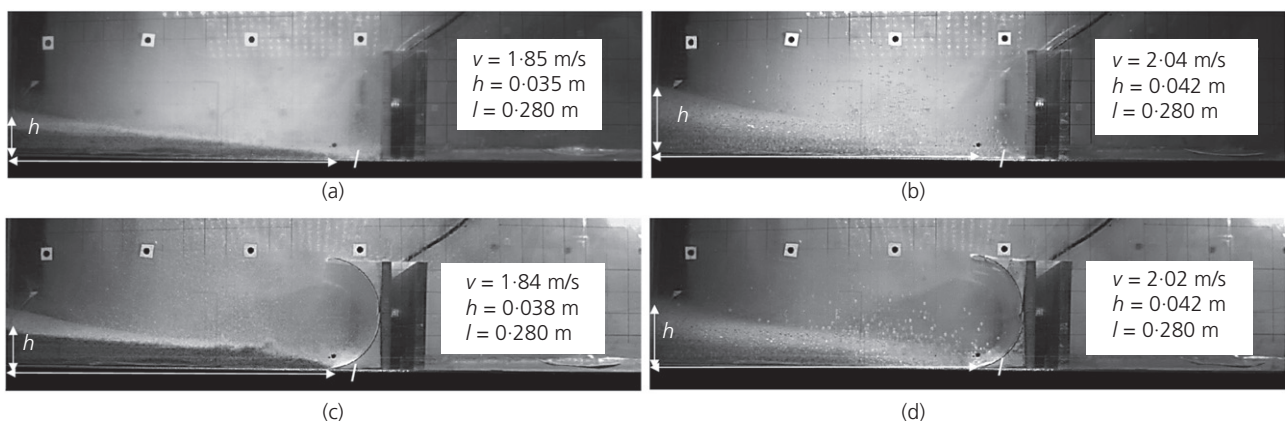
For the curved barrier (test C-G3-I40), the flow front approaches with a maximum velocity of 2.02 m/s at  $t = 10.0$  s (Fig. 7(a)). The granular flow impacts the curved barrier and is guided along the curved surface. A jet begins to form at the top of the curvature and is rebounded towards the upstream direction at 10.2 s (Fig. 7(b)). The contact time between the flow front and the barrier is prolonged by 0.1 s compared to the vertical barrier as momentum is redirected

along a longer curvilinear path. The redirected flow exits the curvature towards the upstream direction at 10.4 s (Fig. 7(c)). The velocity has attenuated by 20% compared to the initial. Subsequent flow deposits underneath the crest of the barrier to form a dead zone and the maximum runup height is achieved at  $t = 10.8$  s (Fig. 7(d)). Once the retention volume is reached, subsequent flow cascades over the barrier at  $t = 11.2$  s (Fig. 7(e)). The velocity of the granular flow is reduced by 37% ( $(2.02 - 1.47 \text{ m/s}) / 1.47 \text{ m/s} = 37\%$ ) compared to the initial velocity. Impact kinematics observed for the curved barrier resembles that observed for waves interacting with curved seawall (Kamikubo *et al.*, 2001; Pearson *et al.*, 2004; Nalarsih, 2015). This demonstrates the effectiveness of curved barriers in mitigating geophysical flows and thus geophysical flows made of granular materials.

A comparison between barrier types shows that a vertical barrier requires the formation of a ramp-like dead zone comprising granular material to transfer momentum vertically along the barrier as shown in Fig. 6(b). By contrast, a curved barrier relies on the geometry of the barrier base to redirect momentum along the curvature as shown in Fig. 7(b). Furthermore, a curved barrier requires 33% longer duration to reach maximum retention capacity compared with a vertical barrier as shown in Table 4. The observed runup mechanism for a vertical barrier launches particles vertically without control. By contrast, the curved barrier directs the flow along the curvature and back towards the approaching flow to facilitate further energy dissipation. The oblique impact between flow front and curved barrier enables longer contact time compared to a vertical barrier. Observations from this study are consistent with that reported by Gupta & Madhu (1992), and Arakawa *et al.* (2006) where oblique impact leads to a longer contact duration, and correspondingly lower impact force.

#### Comparison of dynamic load coefficient

Figure 8 shows the dynamic load coefficient ( $\alpha$ ) for flow impacting vertical and curved barriers with Froude number in the range of 4.7–6.4. Findings from Hungr *et al.* (1984), Faug (2015a) and Cui *et al.* (2015) are shown for comparison. The results show that as Fr increases,  $\alpha$  decreases. This trend agrees with analytical curves from Faug (2015a) and Cui *et al.* (2015). This implies that for granular flows with Fr in the range of 4.7–6.4, the impact force is not solely dependent on velocity. The analytical solution of Faug *et al.* (2012) and Faug (2015a, 2015b) provides more rational  $\alpha$  values whose discrepancy with

**Fig. 5.** Developed flow front for (a) test V-L06-I40; (b) test V-G3-I40; (c) test C-L06-I40; (d) test C-G3-I40

**Table 2.** Physical properties of granular material

Material	Leighton Buzzard Fraction C sand	Glass sphere
Particle diameter: mm	0.6	3
Interface friction angle: °	22.6	22.3
Solid density: kg/m <sup>3</sup>	2650	2570
Bulk density: kg/m <sup>3</sup>	1680	1600

measured results are within 13% compared to the empirical method, which regards  $\alpha$  as a constant. However, the results show that  $\alpha$  for a curved barrier is lower than that of a vertical barrier by up to 25% ( $(0.721-0.542)/0.541 = 0.25$ ) for tests conducted with coarse particles at 40° inclination. This is because the curved surface enables an oblique impact orientation (Arakawa *et al.*, 2006, 2009), elongates the contact duration between flow and barrier by up to 15% (Table 4). The results also show that as Fr increases, the difference in  $\alpha$  between the vertical and curved barriers also increases from 0 to 0.044 for finer particles, and from 0.103 to 0.179 for coarser particles. The change of  $\alpha$  for coarse particles is larger compared to that of the fine particles by about 172%. This indicates that a curved barrier performs better when mitigating flows with coarser particles. This is because the granular flow is composed of finer particles, which are more compressible and any change in geometry has less influence. An assembly of irregular sand grains can exhibit a finite bulk elastic compressibility because some porosity change can be accommodated by elastic shear distortions of angular grain contacts. In contrast, an assembly of rigid spheres in contact with one another has no elastic component of compressibility because any volume change must be accommodated by irreversible slip at grain contacts (Iverson, 2015).

#### Comparison of normalised runup height

Figure 9 shows a comparison of the normalised runup height between the vertical and curved barriers under different Fr by varying the channel inclination from 20° to 40°. The energy principle (Kwan, 2012) and momentum-based approach proposed by Jóhannesson *et al.* (2009) are shown for comparison. The measured results show that the

normalised runup height of granular flow increases with Fr (Choi *et al.*, 2015; Ng *et al.*, 2017b). The normalised runup height of curved barriers is lower compared to an equivalent vertical barrier by about 11% for finer particles and 29% for coarser particles. Runup results show that the curved barrier more effectively mitigates runup (Kamikubo *et al.*, 2003; Anand & Sundar 2016). The results show that as flows become more inertial or Fr increases, the difference between the normalised runup height of the vertical and curved barriers increases by 186% for finer particles, and increases by 338% for coarser particles. This further corroborates that curved barriers more effectively suppress the performance of granular flow that are more inertial, or with higher Fr, and are able to take advantage of the curved geometry. Less inertial flows have a more dominating gravitational component that is more likely to deposit at the base of the barrier.

#### Comparison of regime transition path

Figure 10 shows the granular pattern transition when granular flows interacting with (tests V-G3-I40 and C-G3-I40) curved barriers (test) from  $t = 10.0$  s to  $t = 11.0$  s. The analytical solutions derived by Faug (2015b) are used to characterise the granular patterns. The time of each data point corresponds to the time of snapshots in Figs 4 and 5. The arrow denotes the time sequence. For both vertical and curved barriers, the granular patterns transit from an airborne jet regime to a dead zone regime as the impact process progresses. However, for the curved barrier, a reduction of Fr is more evident compared to a vertical barrier. Therefore, the transition of granular pattern for the curved barrier is more reminiscent of a dead zone regime. This might be caused by that the rebounded jet reduces the inertial component of subsequent flow thus further reducing the Froude number. Results evidently show that curved barrier can prompt a transition of regimes from an airborne jet regime to a dead zone regime and suppress the runup of granular flow.

## CONCLUSIONS

A series of flume experiments were conducted to study the impact mechanism of granular flows against a curved

**Table 3.** Test programme

Test type	Test ID*	Test material	Particle size $\delta$ : mm	Channel inclination $\theta$ : °
Control test: Free flow	F-L06-I20	Leighton Buzzard sand	0.6	20
	F-L06-I30			30
	F-L06-I40			40
	F-G3-I20	Glass sphere	3.0	20
	F-G3-I30			30
	F-G3-I40			40
Impact test: Vertical barrier	V-L06-I20	Leighton Buzzard sand	0.6	20
	V-L06-I30			30
	V-L06-I40			40
	V-G3-I20	Glass sphere	3.0	20
	V-G3-I30			30
	V-G3-I40			40
Impact test: Curved barrier	C-L06-I20	Leighton Buzzard sand	0.6	20
	C-L06-I30			30
	C-L06-I40			40
	C-G3-I20	Glass sphere	3.0	20
	C-G3-I30			30
	C-G3-I40			40

\*F-L06-I20: C denotes the test type: free flow/vertical barrier/curved barrier; L06 denotes the characteristic particle size 0.6/3 mm; I20 denotes the channel inclination: 20/30/40°.

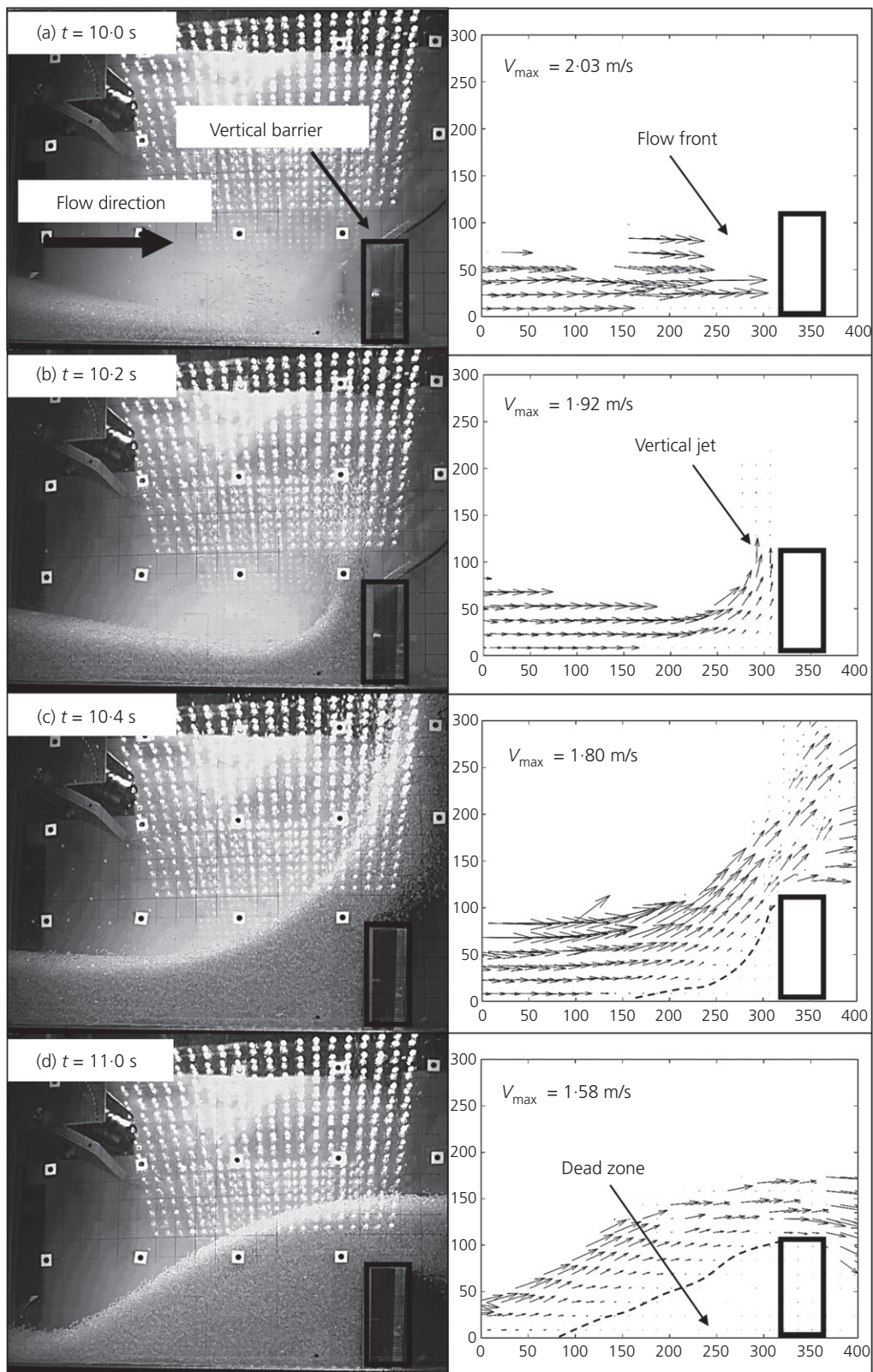


**Fig. 6.** Observed kinematics and PIV analysis for interaction between granular flow and vertical barrier (test V-G3-I40): (a)  $t = 10.0$  s; (b)  $t = 10.2$  s; (c)  $t = 10.4$  s; (d)  $t = 11.0$  s

barrier. The performance of curved barriers was compared against vertical barriers under different  $Fr$ . Findings are as follows:

(a) In comparison to a vertical barrier, curved barriers reduce the runup height and elongate the impact duration by up to 17 and 15%, respectively.

(b) For both vertical and curved barriers, the back-calculated dynamic load coefficient ( $\alpha$ ) decreases when the Froude number is increased. Curved barriers are most suitable for reducing the impact force and suppressing runup height inertial flows, specifically  $Fr > 6.4$  in this study.

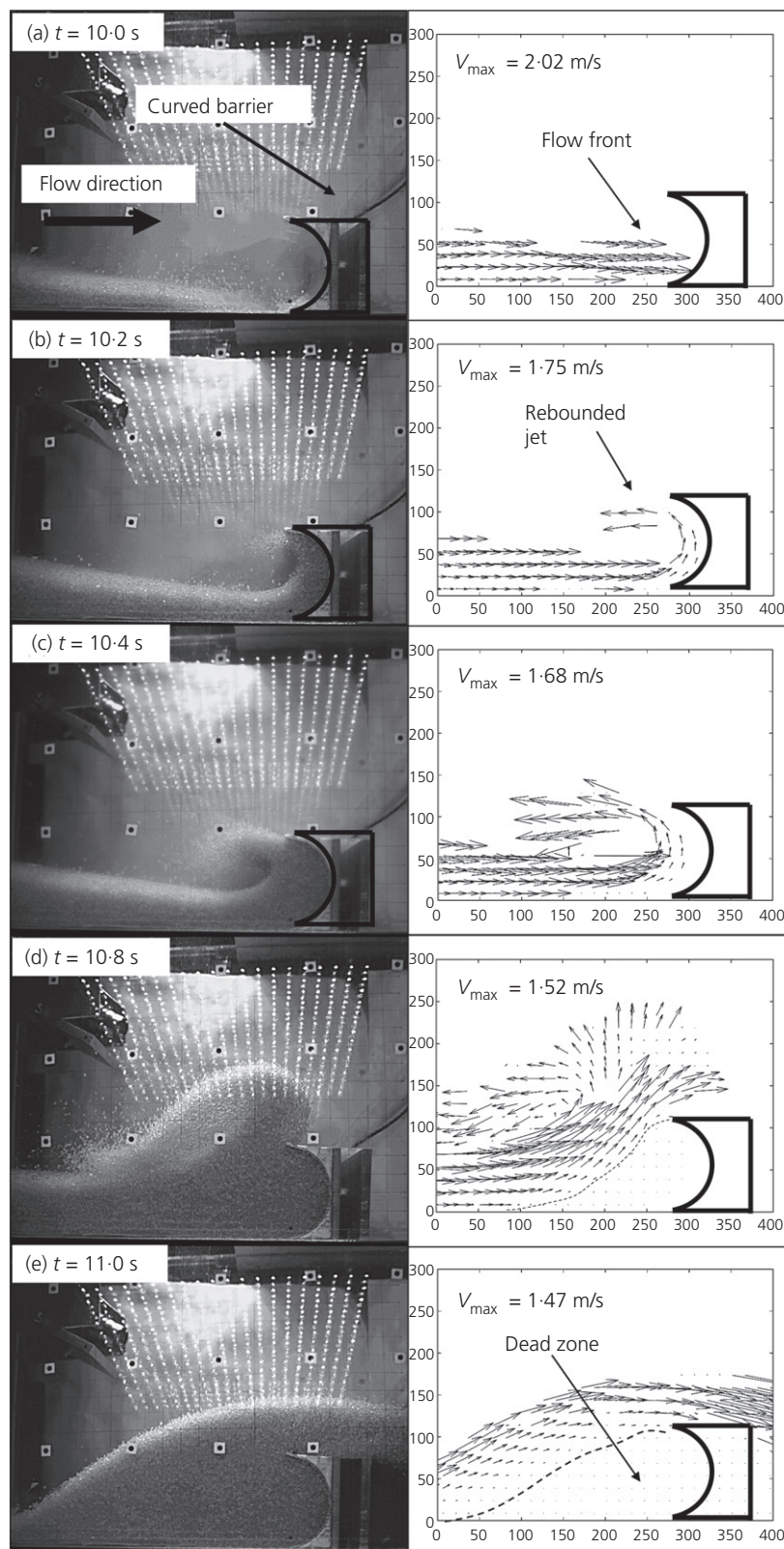


**Fig. 7.** Observed kinematics and PIV analysis for interaction between granular flow and curved barrier (test C-G3-I40): (a)  $t = 10.0$  s; (b)  $t = 10.2$  s; (c)  $t = 10.4$  s; (d)  $t = 10.8$  s; (e)  $t = 11.0$  s

- (c) For curved barriers, the impact force is reduced by up to 25% for coarser granular flows ( $\delta/h = 0.1$ ). By contrast, the impact force does not exhibit a significant reduction for finer granular flows ( $\delta/h = 0.02$ ). This is attributed to the higher compressibility of the finer particles and any change of geometry has less influence on impact force.
- (d) The curved barrier can prompt the granular flow at high Froude number transiting from airborne jets regime to dead zone regime given the rebounded jet might mitigate the inertial component of subsequent flow thus reducing the Froude number.
- (e) Curved barriers show promising engineering value for mitigating geophysical flows and offer potential for

**Table 4.** Duration of impact process

Test ID	Time of front impacting $T_p$ : s	Time of reaching static force $T_s$ : s	Duration of impact process $T = T_s - T_p$
V-L06-I20	27.4	32.7	5.3
V-L06-I30	23.91	27.65	3.74
V-L06-I40	21.79	24.6	2.81
V-G3-I20	17.99	20.48	2.49
V-G3-I30	13.86	15.73	1.87
V-G3-I40	10.06	11.93	1.87
C-L06-I20	27.65	33.27	5.62
C-L06-I30	24.53	28.72	4.19
C-L06-I40	21.41	24.65	3.24
C-G3-I20	17.85	24.4	6.55
C-G3-I30	14.11	19.1	4.99
C-G3-I40	10.06	12.25	2.19

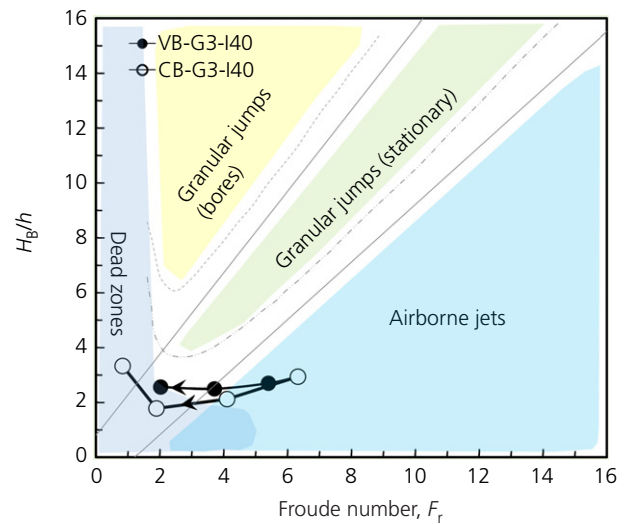


**Fig. 10.** Regime transition path for granular flow-barrier interaction from  $t = 10.0$  s to  $t = 11.0$  s (tests C-G3-I40 and V-G3-I40). The phase diagram is identified by Faug (2015b) using analytical solutions of depth-average approach

optimising designs of existing barriers by reducing both impact capacity and barrier height.

**ACKNOWLEDGEMENTS**

The authors are grateful for financial support from research grant T22-603/15-N provided by the Research Grants Council of the Government of Hong Kong SAR, China and the HKUST Jockey Club Institute for Advanced Study.

**REFERENCES**

Albaba, A., Lambert, S. & Faug, T. (2017). Dry granular avalanche impact force on a rigid wall of semi-infinite height. In *EPJ web of conferences powders and grains 2017 – 8th international conference on micromechanics on granular media*, vol. 140, p. 03054. Les Ulis, France: EDP Sciences.

Arakawa, K., Mada, T., Komatsu, H., Shimizu, T., Satou, M., Takehara, K. & Etoh, G. (2006). Dynamic contact behavior of a golf ball during an oblique impact. *Exp. Mech.* **46**, No. 6, 691–697.

Arakawa, K., Mada, T., Komatsu, H., Shimizu, T., Satou, M., Takehara, K. & Etoh, G. (2009). Dynamic deformation behavior of a golf ball during normal impact. *Exp. Mech.* **49**, No. 4, 471–477.

Armanini, A., Larcher, M. & Odorizzi, M. (2011). Dynamic impact of a debris flow front against a vertical wall. In *Proceedings of 5th international conference on debris flow hazards: mitigation, mechanics, prediction and assessment, Padua, Italy*, pp. 1041–1049.

Anand, K. V. & Sundar, V. (2016). Dynamic pressures and run-up on vertical and curved seawall under random waves. In *Proceeding 12th International Conference on Hydrodynamics ICHD 2016, Egmond aan Zee, the Netherlands*.

Choi, C. E., Au-Yeung, S. C. H., Ng, C. W. & Song, D. (2015). Flume investigation of landslide granular debris and water runup mechanisms. *Geotech. Lett.* **5**, No. 1, 28–32, <http://dx.doi.org/10.1680/geolett.14.00080>.

Choi, C. E., Ng, C. W. W., Goodwin, G. R., Liu, L. H. D. & Cheung, W. W. (2016). Flume investigation of the influence of rigid deflector angle on dry granular overflow mechanisms. *Can. Geotech. J.* **53**, No. 10, 1751–1759.

De Rouck, J., Van de Walle, B. & Geeraerts, J. (2004). Crest level assessment of coastal structures by full scale monitoring, neural network prediction and hazard analysis on permissible wave overtopping. In *European Conference on Marine Science & Ocean Technology 2004, Galway, Ireland*, pp. 261. Luxembourg: Office for Official Publications of the European Communities.

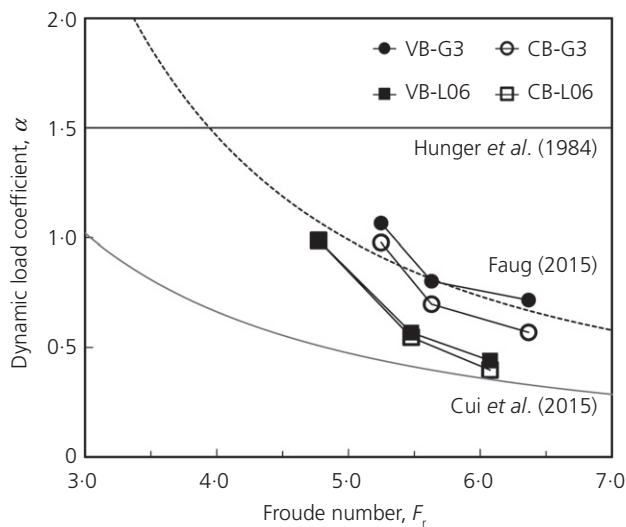


**Fig. 8.** Dynamic load coefficient  $\alpha$  between vertical and curved barriers: reference lines are drawn with  $\alpha = C^* + (K^*/Fr^2)$ , ( $C^*, K^*$ ) = (0.15, 21) (Faug et al., 2012; Faug, 2015a);  $\alpha = 5.3Fr^{-1.5}$  (Cui et al., 2015) and  $\alpha = 1.5$  (Hungr et al., 1984)

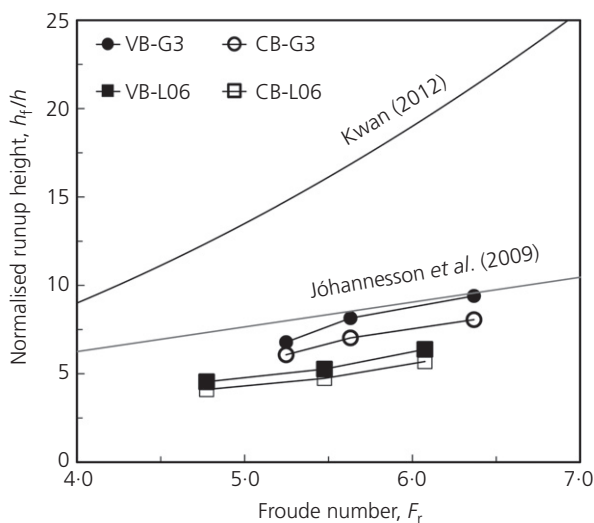


**Fig. 9.** Comparison of normalised runup heights  $h_r/h$  between vertical barrier and curved barriers

- Cui, P., Zeng, C. & Lei, Y. (2015). Experimental analysis on the impact force of viscous debris flow. *Earth Surf. Process. Landforms* **40**, No. 12, 1644–1655.
- EurOtop (2016). Manual on Wave Overtopping of Sea Defences and Related Structures. An Overtopping Manual Largely based on European Research, but for Worldwide Application, Allsop, N. W. H., Bruce, T., DeRouck, J., Kortenhaus, A., Pullen, T., Schüttrumpf, H., Troch, P., van der Meer, J. W. & Zanuttigh, B. See <http://www.overtopping-manual.com> (accessed 27/11/2017).
- Faug, T. (2015a). Macroscopic force experienced by extended objects in granular flows over a very broad Froude-number range. *Eur. Phys. J. E* **38**, No. 5, 34.
- Faug, T. (2015b). Depth-averaged analytic solutions for free-surface granular flows impacting rigid walls down inclines. *Phys. Rev. E* **92**, No. 6, 062310.
- Faug, T., Lachamp, P. & Naaim, M. (2002). Experimental investigation on steady granular flows interacting with an obstacle down an inclined channel: study of the dead zone upstream from the obstacle. Application to interaction between dense snow avalanches and defence structures. *Natural Hazards Earth System Sci.* **2**, No. 3/4, 187–191.
- Faug, T., Caccamo, P. & Chanut, B. (2012). A scaling law for impact force of a granular avalanche flowing past a wall. *Geophys. Res. Lett.* **39**, No. 23, L23401, <http://dx.doi.org/10.1029/2012GL054112>.
- Forterre, Y. & Pouliquen, O. (2011). Granular flows. In *Glasses and Grains* (eds B. Duplantier, T. Halsey and V. Rivasseau), vol. 61, pp. 77–109. Basel, Switzerland: Springer.
- Gupta, N. K. & Madhu, V. (1992). Normal and oblique impact of a kinetic energy projectile on mild steel plates. *Int. J. Impact Engng* **12**, No. 3, 333–343.
- Gray, J. M. N. T., Tai, Y. C. & Noelle, S. (2003). Shock waves, dead zones and particle-free regions in rapid granular free-surface flows. *Journal of Fluid Mechanics* **491**, 161–181, <http://dx.doi.org/10.1017/S0022112003005317>.
- Hübl, J., Suda, J., Proské, D., Kaitna, R. & Scheidl, C. (2009). Debris flow impact estimation. In *Proceedings of the 11th international symposium on water management and hydraulic engineering*, pp. 1–5. Ohrid, Macedonia: ISWHE.
- Hungr, O., Morgan, G. C. & Kellerhals, R. (1984). Quantitative analysis of debris torrent hazards for design of remedial measures. *Can. Geotech. J.* **21**, No. 4, 663–677.
- Iverson, R. M. (2015). Scaling and design of landslide and debris-flow experiments. *Geomorphology* **244**, 9–20, <https://doi.org/10.1016/j.geomorph.2015.02.033>.
- Iverson, R. M. & George, D. L. (2014). A depth-averaged debris-flow model that includes the effects of evolving dilatancy. I. Physical basis. *Proc. Roy. Soc.* **470**, No. 2170, 20130819.
- Iverson, R. M. & Vallance, J. W. (2001). New views of granular mass flows. *Geology* **29**, No. 2, 115–118.
- Jóhannesson, T., Gauer, P., Issler, P., Lied, K. & Hákonardóttir, K. M. (2009). *The design of avalanche protection dams: recent practical and theoretical developments*. Brussels, Belgium: European Commission.
- Kamikubo, Y., Murakami, K., Irie, I. & Hamasaki, Y. (2001). Study on practical application of a non-wave overtopping type seawall. *Coastal Eng.* **2000**, 2215–2228, [https://doi.org/10.1061/40549\(276\)173](https://doi.org/10.1061/40549(276)173).
- Kamikubo, Y., Murakami, K., Irie, I., Kataoka, Y. & Takehana, N. (2003). Reduction of wave overtopping and water spray with using flaring shaped seawall. In *Proceedings of the 13th international offshore and polar engineering conference, Honolulu, HI, USA*, vol. 3, No. 1, pp. 671–676.
- Koo, R. C. H., Kwan, J. S., Ng, C. W. W., Lam, C., Choi, C. E., Song, D. & Pun, W. K. (2017). Velocity attenuation of debris flows and a new momentum-based load model for rigid barriers. *Landslides* **14**, No. 2, 617–662.
- Kwan, J. S. H. (2012). *Supplementary technical guidance on design of rigid debris-resisting barriers*, Technical Note No. TN 2/2012. Hong Kong, China: Geotechnical Engineering Office, Civil Engineering and Development Department.
- Mizuyama, T. (1979). Estimation of impact force on dam due to debris flow and its problems. *J. Japan Soc. Erosion Control Engng* **112**, No. 1, 40–43.
- Nalarsih, M. (2015). A seawall design with a revetment and the wave reflector to protect coast and maintain the position of maron coast line semarang. In *Proceedings of the International conference on geological and civil engineering*, vol. 80, pp. 57–61. Singapore: IACSIT Press.
- Ng, C. W. W., Song, D., Choi, C., Liu, L. H. D., Kwan, J. S. H., Koo, R. C. H. & Pun, W. K. (2016). Impact mechanisms of granular and viscous flows on rigid and flexible barriers. *Can. Geotech. J.* **54**, No. 2, 188–206.
- Ng, C. W. W., Choi, C. E., Goodwin, G. R. & Cheung, W. W. (2017a). Interaction between dry granular flow and deflectors. *Landslides* **14**, No. 4, 1375–1387.
- Ng, C. W. W., Choi, C. E., Liu, L. H. D., Wang, Y., Song, D. & Yang, N. (2017b). Influence of particle size on the mechanism of dry granular run-up on a rigid barrier. *Geotech. Lett.* **7**, No. 1, 79–89, <http://dx.doi.org/10.1680/jgeot.16.00159>.
- Ng, C. W. W., Choi, C. E., Koo, R. C. H. & Kwan, J. S. H. (2017c). Dry granular flow interaction with dual-barrier systems. *Geotechnique* **1**, No. 14, <https://doi.org/10.1680/jgeot.16.P.273>.
- Pearson, J., Bruce, T., Allsop, W., Kortenhaus, A. & van der Meer, J. (2004). Effectiveness of recurve walls in reducing wave overtopping on seawalls and breakwaters. In *Coastal engineering*, pp. 4404–4416. Singapore: World Scientific Publishing.
- Song, D., Ng, C. W. W., Choi, C., Zhou, G. G., Kwan, J. S. H. & Koo, R. C. H. (2017). Influence of debris flow solid fraction on rigid barrier impact. *Can. Geotech. J.* **54**, No. 10, 1421–1434.
- Thorn, R. B. & Roberts, A. G. (1981). *Sea defence and coast protection works: a guide to design*. London, UK: Thomas Telford.
- VanDine, D. F. (1996). *Debris flow control structures for forest engineering*. Victoria, BC, Canada: Ministry of Forests Research Program.
- White, D. J., Take, W. A. & Bolton, M. D. (2003). Soil deformation measurement using particle image velocimetry (PIV) and photogrammetry. *Geotechnique* **53**, No. 7, 619–631, <https://doi.org/10.1680/geot.2003.53.7.619>.
- Zhou, G. G. & Ng, C. W. (2010). Dimensional analysis of natural debris flows. *Can. Geotech. J.* **47**, No. 7, 719–729.

#### HOW CAN YOU CONTRIBUTE?

To discuss this paper, please submit up to 500 words to the editor at [journals@ice.org.uk](mailto:journals@ice.org.uk). Your contribution will be forwarded to the author(s) for a reply and, if considered appropriate by the editorial board, it will be published as a discussion in a future issue of the journal.